

## Article

# Additively Manufactured Transverse Flux Machine Components with Integrated Slits for Loss Reduction

Thomas Kresse <sup>1,\*</sup>, Julian Schurr <sup>1</sup>, Maximilian Lanz <sup>1</sup>, Torsten Kunert <sup>1</sup> , Martin Schmid <sup>2</sup> , Nejila Parspour <sup>2</sup>, Gerhard Schneider <sup>1</sup> and Dagmar Goll <sup>1</sup>

<sup>1</sup> Materials Research Institute, Aalen University, 73430 Aalen, Germany

<sup>2</sup> Institute of Electrical Energy Conversion, University of Stuttgart, 70569 Stuttgart, Germany

\* Correspondence: thomas.kresse@hs-aalen.de; Tel.: +49-7361-576-1622

**Abstract:** Laser powder bed fusion (L-PBF) was used to produce stator half-shells of a transverse flux machine from pure iron (99.9% Fe). In order to reduce iron losses in the bulk components, radially extending slits with a nominal width of 150 and 300  $\mu\text{m}$ , respectively, were integrated during manufacturing. The components were subjected to a suitable heat treatment. In addition to a microscopic examination of the slit quality, the iron losses were also measured using both a commercial and a self-developed measurement setup. The investigations showed the iron losses can be reduced by up to 49% due to the integrated slits and the heat treatment.

**Keywords:** additive manufacturing; selective laser melting (SLM); laser powder bed fusion (L-PBF); transverse flux machine components; soft magnets; loss reduction



**Citation:** Kresse, T.; Schurr, J.; Lanz, M.; Kunert, T.; Schmid, M.; Parspour, N.; Schneider, G.; Goll, D. Additively Manufactured Transverse Flux Machine Components with Integrated Slits for Loss Reduction. *Metals* **2022**, *12*, 1875. <https://doi.org/10.3390/met12111875>

Academic Editor: Tadeusz Kulik

Received: 26 September 2022

Accepted: 30 October 2022

Published: 3 November 2022

**Publisher's Note:** MDPI stays neutral with regard to jurisdictional claims in published maps and institutional affiliations.



**Copyright:** © 2022 by the authors. Licensee MDPI, Basel, Switzerland. This article is an open access article distributed under the terms and conditions of the Creative Commons Attribution (CC BY) license (<https://creativecommons.org/licenses/by/4.0/>).

## 1. Introduction

As a consequence of progressive efficiency improvements in energy conversion, high-inductance, low-loss soft magnet components are desirable for high-torque electrical machines used at high frequencies. Most soft magnetic components used today are made of either rolled electrical steel or soft magnetic composite (SMC) materials. However, there exist limits to the desired component geometry due to their mechanical properties and manufacturing-related material shape. Depending on the desired component geometry, even material improvement with regard to the magnetic and mechanical properties cannot fully compensate these limitations. As a result, more complex components may only be manufactured at great expense in terms of time and money.

Additive manufacturing offers new opportunities in this respect: The manufacturing method allows the use of further materials, e.g., electrical steel with higher Si content for higher electrical resistance, that until now have rarely been used due to their difficult, complex and cost-intensive production in order to overcome inadequate ductility and limited formability [1]. The method also offers greater design freedom [2–5]. This enables material- and weight-saving designs and thus improved component dynamics, such as shorter start-up time of electric motors without compromising mechanical stability [6–8]. Another possibility for component optimization is the integration of cavities and slits in the volume that spatially limit the eddy currents and thus reduce the iron losses compared to the bulk material [2,9,10] and increase the electromagnetic efficiency of the component. Thus, the production of special components with optimized soft magnetic properties for the respective special application in electrical machines is possible [11,12].

One possible use case for L-PBF additively manufactured magnetic circuit components is the transverse flux machine (TFM) [13–15]. In this design, the magnetic flux runs along the axis of rotation and to the current flowing through an annular coil arranged around the axis of rotation. Such a component is characterized by both high torque density and relatively high torque at low speeds. This makes it very suitable for direct drive applications,

such as in traction motors for electric vehicles [14]. Another advantage of this design is the decoupling of the magnetic and electric circuits, which allows independent dimensioning of the two components [14]. However, a transverse flux machine requires a more complex geometry than conventional radial axis machines. Furthermore, due to the magnetic flux guidance, laminated electrical steels, which are normally the preferred construction material of conventional radial axis machines [13,14], cannot be used. Therefore, the common transverse flux machines are usually made of sintered soft magnetic composites (SMCs) [16,17]. SMCs have low iron losses at high frequencies but also low magnetic moment densities, which in turn require more component volume in the design [15]. Moreover, SMCs exhibit low permeabilities, low mechanical strengths and high coercivities leading to high hysteresis losses. In addition, the overall component must be assembled from several sintered individual parts [14]. Secondly, powder metallurgical processes are not suitable for all sizes and highly complex shapes of soft magnetic cores [18].

Additive manufacturing, on the other hand, allows the fabrication of the entire component in fewer construction steps using better suited magnetic materials (e.g., with high electrical resistance and relatively high induction) such as Fe-6.7%Si [1]. The present publication is intended to show the feasibility in principle of loss reduction by means of laser-assisted additive manufacturing as well as the verification of loss reduction by means of non-destructive magnetic characterization methods using the application example of a stator of a transverse flux machine.

A suitable slit configuration for the component to be optimized was found by means of simulation. This configuration, as well as comparable reference samples, was then realized by additive manufacturing. Subsequently, the components were characterized with regard to the build and process quality as well as the soft magnetic properties in order to demonstrate the feasibility and potential of additive manufacturing of electric machine components.

## 2. Materials and Methods

### 2.1. Simulation

The stator to be manufactured consists of two identical half-shells, the approximate shape of which has already been determined in earlier works using finite element (FEM) simulations [19–21]. At that time, SMC powder was used as the starting material to limit the high eddy current losses of the massive components. However, soft magnet composites have disadvantages with regard to their mechanical and magnetic properties, such as brittleness and relatively low saturation polarization.

In this work, pure iron (99.9%), which has a high saturation polarization but a relatively high conductivity, is used. Therefore, to avoid too high eddy currents, FEM simulations were performed integrating slits of different width and number into the component. In the simulation performed by means of the software COMSOL Multiphysics 5.6/6.0 (COMSOL AB, Stockholm, Sweden), only one pole of a phase (i.e., 1/12 of a whole half-shell) has been considered. This is possible due to the magnetic decoupling of the individual phases of the transverse flux machine arranged axially one behind the other, as well as the assumption of perfect symmetry within a phase. This reduction of the model is necessary to be able to perform the time-consuming transient summations that are necessary for the consideration of the eddy current losses. For the simulation, an operating point at a speed of  $1100 \text{ min}^{-1}$  has been investigated.

The simulation showed that a significant increase in efficiency is achieved by the insertion of at least four slits per pole due to the reduction of eddy current losses. Figure 1 shows the simulated spatial distribution of the volumetric loss density in one pole of a stator half-shell both with and without integrated slits. A reduction in the shown loss density due to the slits below and next to the ring winding is clearly visible. An insertion of more than four slits only leads to slight improvements in the degree of efficiency. However, the increase in the numbers of slits successively decreases the magnetic flux within the whole machine because of the decrease of magnetic material in the component volume.

Therefore, a configuration with four slits per pole has been chosen because it represents a good compromise between sufficiently high magnetic flux and sufficiently low iron losses. The final stator half-shells had a diameter of 42.0 mm, a height of 10.8 mm, a bar width of 1.0 mm, 12 pole pairs each and 48 slits each of different widths between 50 and 500  $\mu\text{m}$ .

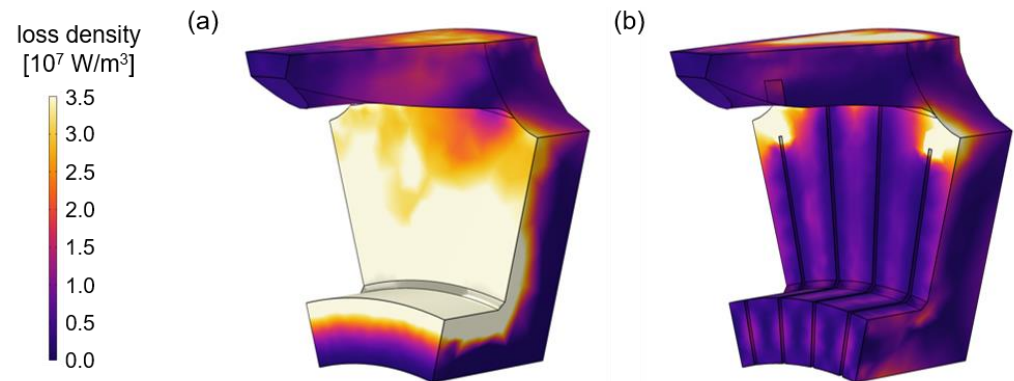


**Figure 1.** Simulated spatial distribution of the electromagnetic loss density per unit volume within a pole of the stator half-shell to be manufactured. (a) Pole without integrated slits. (b) Pole with 4 integrated slits.

## 2.2. Materials

The transverse flux stators are soft magnetic motor components intended to demonstrate the possibilities of implementing loss-reducing slit geometries. For this reason, unalloyed (pure) iron powder was used (purity 99.9%). The raw material was atomized by NANOVAL GmbH & Co. KG (Berlin, Germany) using the special NANOVAL process. The special feature here is gas atomization by means of a Laval nozzle. This process results in a finer and narrower particle size distribution compared to other atomization processes. In this way, a high yield of atomized material could be achieved. After atomization, the particle size distribution was fractionated to  $+25/-70 \mu\text{m}$  by air classification and sieving.

## 2.3. Additive Manufacturing

The components were produced on a TruPrint1000 Multilaser (max. laser power  $P_L = 200 \text{ W}$ , max. scanning speed  $v_s = 3000 \text{ mm/s}$ ) by TRUMPF SE + Co. KG (Ditzingen, Germany). The process parameters were optimized using a two-stage parameter study. First, a wide range of parameters ( $P_L = 100\text{--}175 \text{ W}$ ;  $v_s = 400\text{--}800 \text{ mm/s}$ ) could be tested for the production of bulk material and subsequently optimized for the additive manufacturing of components with integrated slits. One component without slits (as a reference sample) and two components with slits were produced, with the specified slit widths being 150 and 300  $\mu\text{m}$ , respectively (Figure 2). The slits were realized by not traversing the corresponding areas with the laser. The quality of bulk material and slits was evaluated by optical microscopy analysis. Finally, a compromise between the slit and component quality was chosen with the parameter set  $P_L = 175 \text{ W}$ ;  $v_s = 500 \text{ mm/s}$ ; hatch distance  $h = 90 \mu\text{m}$ ; layer thickness  $t = 20 \mu\text{m}$ . The resulting laser energy density (using a laser spot diameter of 55  $\mu\text{m}$ ) is  $116 \text{ J/mm}^3$ , according to [22]. For the slit widths, the modeled values 150 and 300  $\mu\text{m}$  were used.

In order to remove microstructure defects introduced during the manufacturing process (e.g., inhomogeneities, high grain boundary density, stress, deformation) in the entire solid components, they were subjected to an appropriate heat treatment (1150  $^\circ\text{C}$ , 6 h in an Ar atmosphere with 5%  $\text{H}_2$ ) after initial characterization.

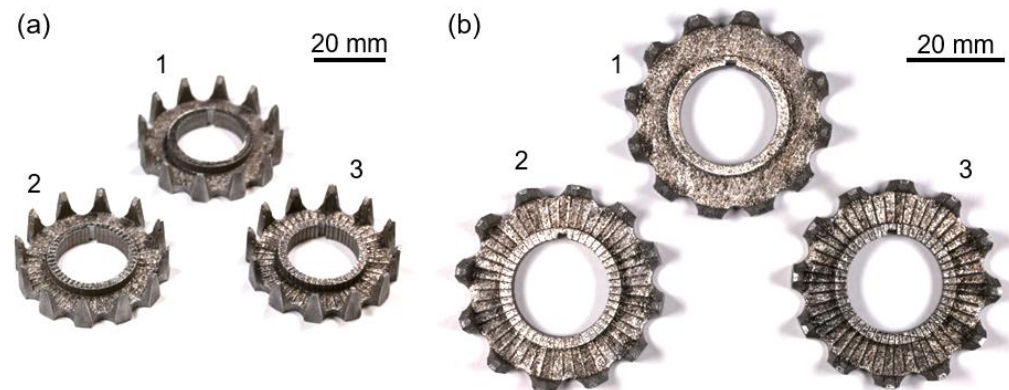


**Figure 2.** Additively manufactured stator half-shells made of 99.9% pure iron, (1) without slits, (2) with 150  $\mu\text{m}$  nominal slit width and (3) with 300  $\mu\text{m}$  nominal slit width. (a) Aerial view. (b) Top view.

#### 2.4. Analysis

The particle size distribution of the powder material used was determined by a HELOS H4299 laser diffraction system (Sympatec GmbH, Clausthal-Zellerfeld, Germany). Imaging analysis of the powder was performed using light (ZEISS Axio Imager Vario) and scanning electron microscopy (ZEISS Sigma 300 VP) by Carl Zeiss Microscopy GmbH (Oberkochen, Germany). A final evaluation of the metal powder was performed using the flowability measurement in a Carney Funnel.

The density of the cubic samples (with an edge length of 10 mm) for the parameter study was measured using Archimedes' principle by means of a AUW220D precision balance (Shimadzu Corp., Kyoto, Japan). The mass of each sample in air and in ethanol was determined for several times.

The component quality of the additively manufactured transverse flux stator half-shells was evaluated using computer tomography (CT) analyses. A CT with micro- and nanofocus tubes (Phoenix v|tome|x s c 240/180, General Electric Company, Boston, MA, USA) was used for this purpose. Based on the CAD data of the printed component, a nominal/actual comparison could thus be made.

A test set-up was developed for non-destructive magnetic component testing. For this purpose, two stator half-shells, each with a centrally mounted coil unit (consisting of primary and secondary coil), were aligned according to their functional arrangement with the aid of a plastic shaft with inserted feather key (Figure 3a). The primary coil is connected to an AC power supply unit, with the corresponding excitation current  $I_{in}$  being measured via a controller (Figure 3b). Frequency-dependent iron losses were specifically analyzed via defined excitation frequencies of 50, 100, 200, 250, 500 and 1000 Hz. In this system setup, the magnetic flux runs along the stator axis, starting from the primary coil (140 turns) through the inner bar radially onto the top and bottom of the samples, where it is deflected by the stator teeth on the outside of the samples. Using a constant primary current  $I_{in}$  of 0.5 A, a constant magnetic flux density of up to 0.8 T is thus achieved in the middle bar of the stator half-shells, according to the simulation. The voltage  $U_{out}$ , which is induced in the secondary coil, is measured by an external voltage sensor and can be considered as a direct measurement of the magnetic behavior of the stator sample. The frequency-independent ratio of  $I_{in}$  and  $U_{out}$

$$R_R = \frac{\left(\frac{U_{out}}{I_{in}}\right)}{f}$$

is the so-called response ratio and is formed analogously to the efficiency (ratio of result to effort). The possible setting parameters of this set-up are the excitation current  $I_{in}$ , the frequency  $f$  and the signal form of the AC current. In this case, a sinusoidal signal has been used.

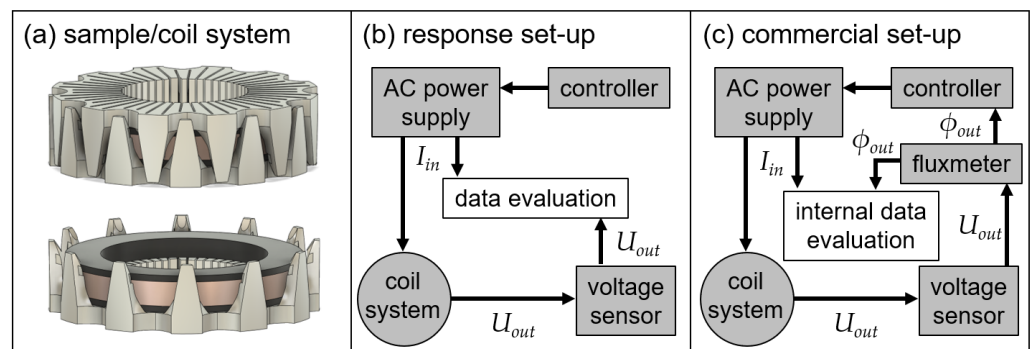


**Figure 3.** Schematic of the measurement set-up for the magnetic analysis of the additively manufactured stator half-shells. (a) Arrangement of the sample and the measurement coil system consisting of a black plastic shaft and the wound primary and secondary coil. (b) Schematic of the commercial measuring device MPG 200 D (Dr. Brockhaus Measurements GmbH). (c) Schematic of the self-constructed measurement set-up.

In addition, the performance in the alternating field was also investigated on a toroidal sensor of a commercial MPG 200 D measuring device (Dr. Brockhaus Measurements GmbH, Lüdenscheid, Germany) designed for standard magnetic measurements, according to IEC 60404-4 and 60404-6. In this set-up, the measurement control as well as the data evaluation is handled by the internal software of the device (Figure 3c). Instead of a constant value, the applied excitation current is determined by the given magnetic polarization of the sample and is adjusted via the resulting magnetic flux  $\phi_{out}$  calculated from the measured voltage  $U_{out}$ . The possible setting parameters for this set-up are the magnetic polarization and the frequency. Due to the deviating measurement arrangement, however, some adjustments had to be made during the measurement. Normally, in this measurement method, the two coils (primary and secondary) are arranged around the ring-shaped sample in such a way that the magnetic flux is exclusively within the material under investigation. In this case, however, the magnetic flux is partially outside the sample. Furthermore, in conventional toroidal measurements, the coil system runs radially around the toroidal axis, whereas in this case it runs parallel to it. For the toroidal geometries to be specified in the measurement program, from which both the field strength  $H$  of the external field and the magnetic polarization  $J$  of the magnetic sample are calculated, values—which would give the same cross-sectional area enclosed by the coil system if the coil system was arranged in the conventional way—were therefore chosen. Measurements were made at frequencies between 100 and 500 Hz at a peak polarization of 0.1 T. The lower polarization compared to the magnetic response investigation was chosen to prevent overheating and thus probable destruction of the thin coil wires.

### 3. Results

#### 3.1. Powder Characterization

The particle size distribution determined by laser diffraction is shown in Figure 4. The  $D_{10}$ ,  $D_{50}$  and  $D_{90}$  values were found to be 26  $\mu\text{m}$ , 41  $\mu\text{m}$  and 60  $\mu\text{m}$ , respectively. The powder is therefore very suitable for the L-PBF process.

The analysis of the powder morphology by scanning electron microscopy shows typical features for gas atomized metal powders. The particles exhibit good sphericity (Figure 5). In some cases, irregularly shaped particles or satellites can be seen, but these have not had a particularly negative effect on the flowability. The flowability measurement of the material powder showed a flow time of 3.58 s per 50 g and a bulk density of 4.04 g/cm<sup>3</sup>.

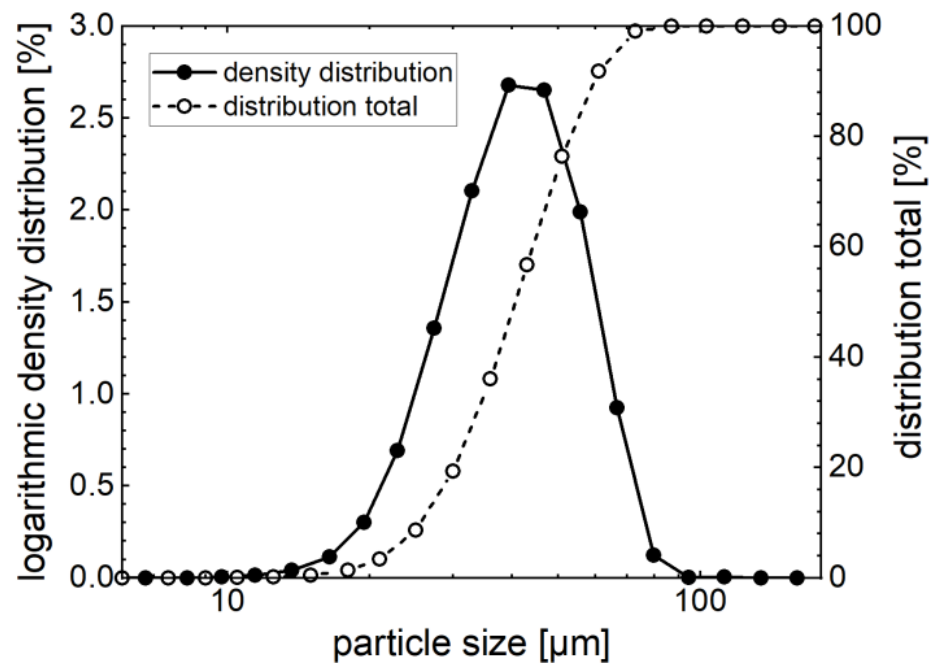


**Figure 4.** Volume-specific particle size distribution of the powder used for additive manufacturing (99.9% pure iron) determined by laser diffraction. The median of the particle size distribution is about 41  $\mu\text{m}$ .

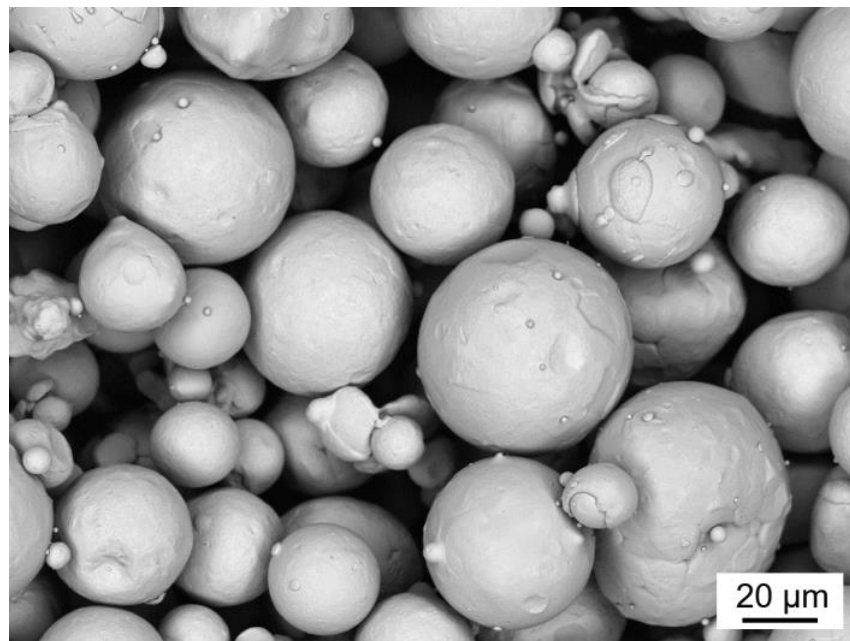


**Figure 5.** SEM image of the powder (99.9% pure iron) taken by backscattered electron detector.

### 3.2. Parameter Study for the Additive Manufacturing Process

The parameter study was analyzed primarily with regard to the density of the specimens. It was found that the density of the specimens decreases with increasing scanning speed (Figure 6). The best results were achieved with the parameter set 175 W, 400 mm/s and a resulting component density of  $7.83 \text{ g/cm}^3$ , which corresponds to a relative density of 99.4% regarding the nominal density of pure iron ( $7.874 \text{ g/cm}^3$ ). Increasing the scanning speed to 500 mm/s leads to a slight reduction of the density to 98.7%.

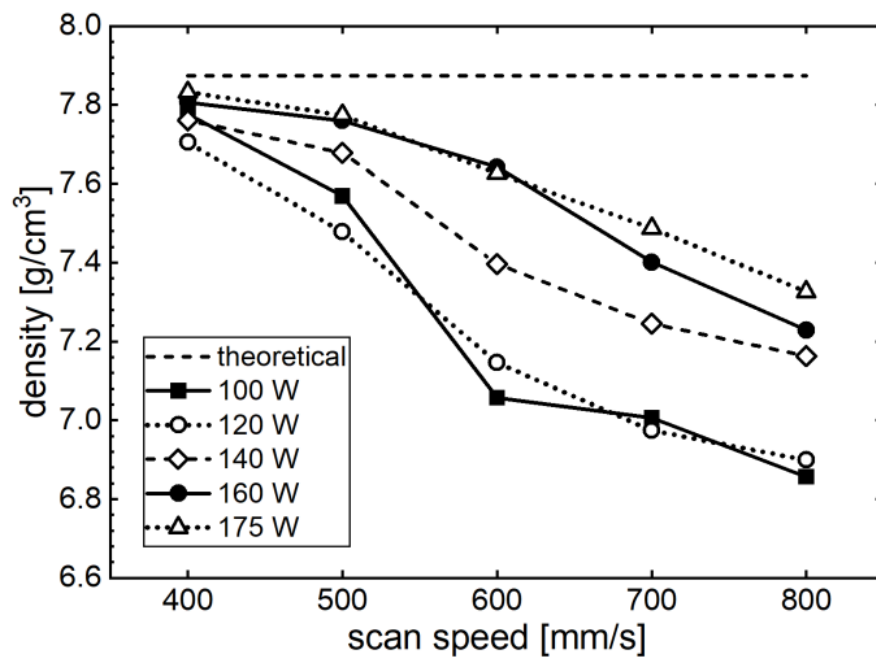


**Figure 6.** Density of additively manufactured specimens made of 99.9% pure iron (as-built) as a function of the scanning speed and laser power used.

### 3.3. Quality of the Inner Surface of the Slits

The analysis of the slits of widths between 50 and 500  $\mu\text{m}$  showed that, only from a modeled slit width above 200  $\mu\text{m}$ , continuous air gaps could be generated (Figure 7). Especially for small slit widths of 100 and 150  $\mu\text{m}$ , the parameter combination  $P_L = 175\text{ W}$  and  $v_s = 500\text{ mm/s}$  showed advantages with respect to slit quality. This is why this parameter set was also used for the final component production. The better quality of the edge and slit areas at  $v_s = 500\text{ mm/s}$  justifies the minimally lower density at  $P_L = 175\text{ W}$ . The components produced, however, had a lower density than those produced at  $v_s = 500\text{ mm/s}$ . However, the manufactured slits tended to have smaller widths than specified in the design. Thus, after additive manufacturing, instead of the nominal slit widths of 150 and 300  $\mu\text{m}$ , the actual slit widths were in the range of 0–100  $\mu\text{m}$  and 75–190  $\mu\text{m}$ , respectively.

An analysis of the slit quality, transferred to the real component geometry, was carried out using CT analyses of additively manufactured individual teeth of a stator half-shell (Figure 8). The modeled slit width of 150  $\mu\text{m}$  corresponds to potentially continuous slits, which may have some singular connections. From a modeled slit width of 300  $\mu\text{m}$ , completely continuous air gaps can be expected.

In order to exclude distortions of the components due to the heat treatment, CT analyses were also carried out on the heat-treated components. A worst-case scenario with a heat treatment temperature of 1450  $^{\circ}\text{C}$  was investigated (Figure 9). The analysis showed that the components exhibit very good dimensional stability, even after annealing at such a high annealing temperature. The slit quality was also not negatively affected by the heat treatment. The high deflections on the underside of the specimen can be explained by edge effects of the CT analysis.

### 3.4. Magnetic Analysis

The component without slits exhibits the lowest response ratio and thus the highest iron losses in the frequency range from 50 to 1000 Hz (Figure 10). By integrating narrow and wide slits, the response ratio  $R_R$  at 50 Hz improves by approx. 9% and 17%, respectively. As frequency increases, the differences in response ratio become more pronounced. At 1000 Hz, for example, the component with narrow or wide slits improves by approx. 15% and 95%, respectively, in relation to the component without slits. The heat treatment significantly increases the response ratio at low frequencies for all three components. At 50 Hz, the

component without slits improves by approx. 16%; the component with narrow slits by approx. 10%; and the component with wide slits by 9%. However, at higher frequencies the improvement is significantly lower. Thus, at an excitation frequency of 1000 Hz, the heat treatment leads to an improvement of only 2.9% for the component with narrow slits; 1.3% for the component with wide slits; and 0.4% for the component without slits.

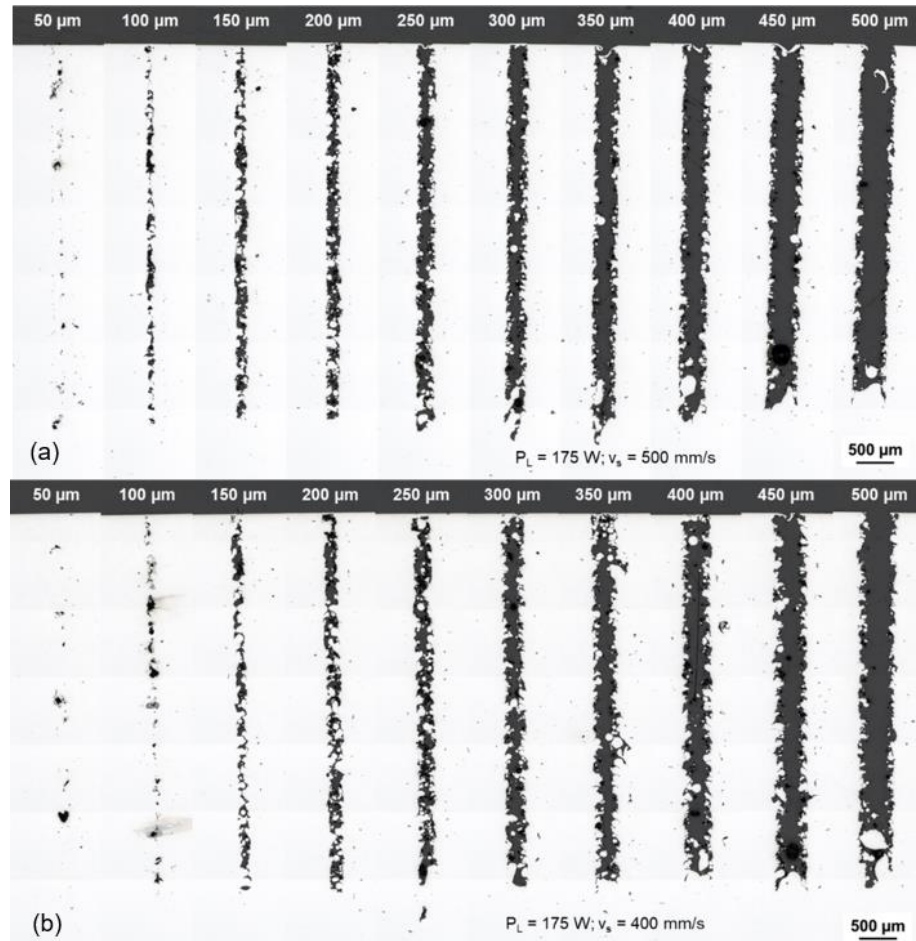


**Figure 7.** Cross-sections of the slits of different widths in the additively manufactured 99.9% pure iron specimen taken by optical microscopy at constant laser power ( $P_L = 175$  W) and different scanning speeds: (a)  $v_s = 400$  mm/s. (b)  $v_s = 500$  mm/s.

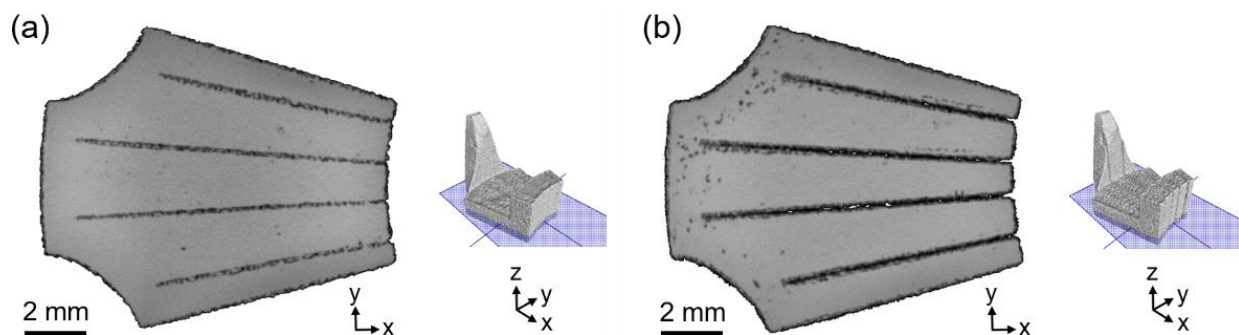


**Figure 8.** CT analysis of additively manufactured individual teeth of a modeled stator half-shell made of 99.9% pure iron with integrated as-built slits. (a) Nominal slit width 150  $\mu$ m. (b) Nominal slit width 300  $\mu$ m.

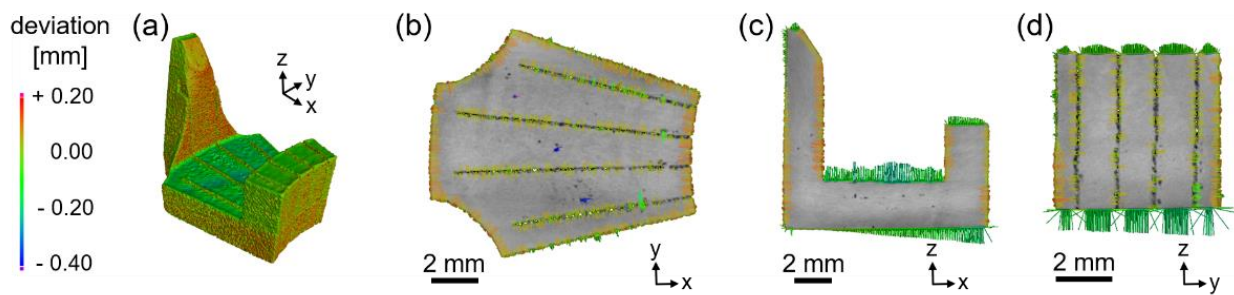


**Figure 9.** CT analysis of an additively manufactured and heat-treated (6 h @ 1450 °C) single tooth of a modeled stator half-shell made of 99.9% pure iron with integrated slits of 150  $\mu\text{m}$  nominal width each. The colored deflections indicate the deviation of the edge geometries from the modeled template. The colored lines in the right subfigures representing the extent of the deviation in the range of  $\pm 150 \mu\text{m}$  are shown enlarged for better illustration. (a) Aerial view. (b) View from above (z direction). (c) View from the side (y direction). (d) View from the side (x direction).

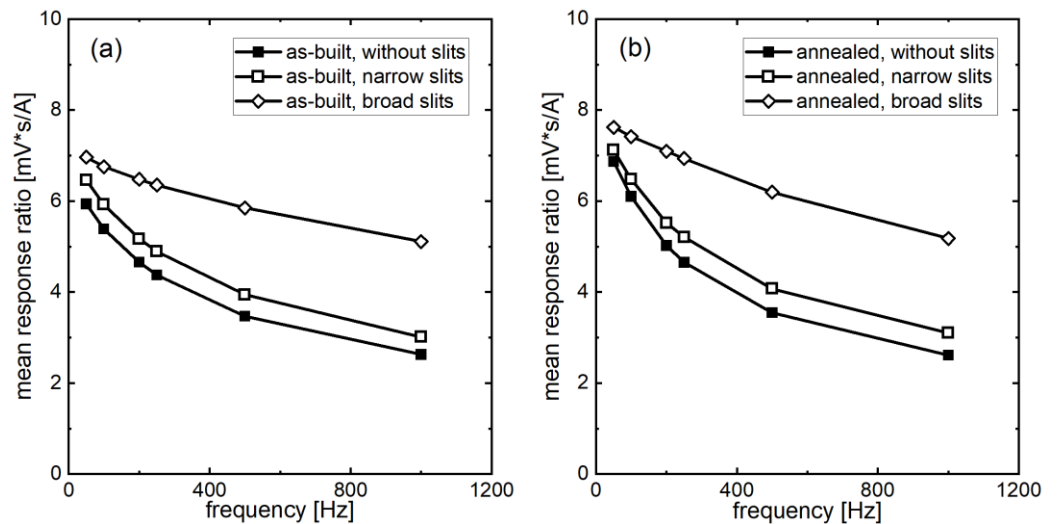


**Figure 10.** Mean response ratio of the 99.9% pure iron stator half-shells investigated using the magnetic response setup as a function of the frequency used. The response ratio is the induced sensor voltage  $U_{out}$  of the secondary coil divided by the excitation current  $I_{in}$  of the primary coil and the applied frequency  $f$ . (a) As-built state. (b) Annealed state (1150 °C; 6 h).

Figure 11 shows the iron losses of the additively manufactured components measured using the commercial soft magnet measuring station. The component without slits exhibits the highest iron loss per unit volume in the considered frequency range. In contrast, the components containing radially arranged slits exhibit lower iron losses. At 500 Hz, losses are about 15% lower for narrow slits and about 57% lower for wide slits. The heat treatment performed generally leads to a significant reduction in iron losses for all three components. In the case of the components without or with only narrow slits, the loss reduction is 48% and 47%, respectively, whereas in the case of wide slits it is only approx. 38%.

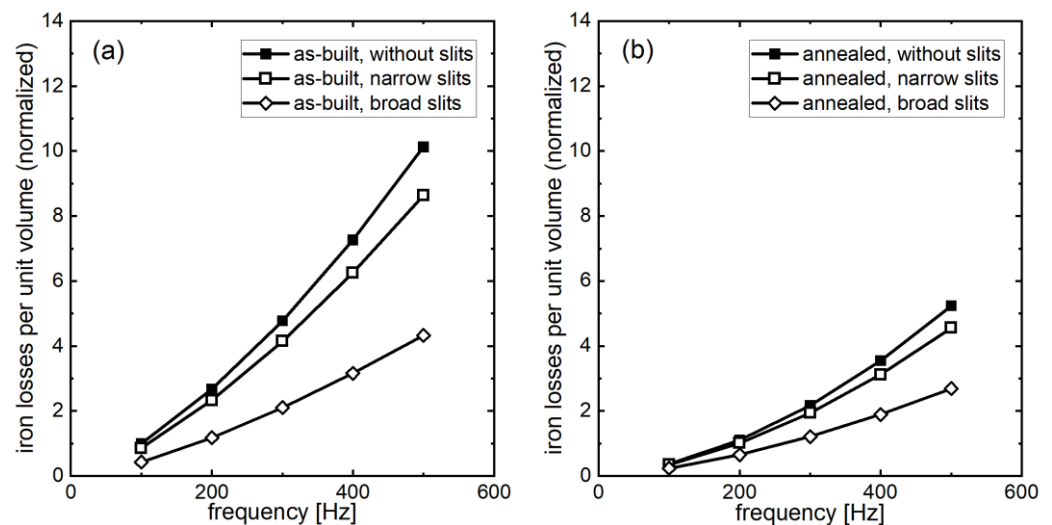


**Figure 11.** Normalized iron losses of the transverse flux components made of 99.9% pure iron at 0.1 T peak polarization, measured with the commercial measuring instrument MPG 200 D (Dr. Brockhaus Measurements GmbH). The reference value (=1) is the iron losses of the as-built compact component at 100 Hz. (a) As-built state. (b) Annealed state (1150 °C; 6 h).

#### 4. Discussion

The additively manufactured components were built up without cracks or external defects (e.g., delamination, excessive surface roughness). The CT analyses also showed that soft magnetic components with integrated slits can be assembled close to final contour with the aid of additive manufacturing. It was furthermore possible to introduce a tailored heat treatment without any deterioration in dimensional accuracy. The resulting slits tended to have slightly smaller widths than predefined in the corresponding CAD model. The reasons for this are both the deliquescence of the locally melted starting material and the extension of the laser focus of approx. 55  $\mu\text{m}$  that results in a smaller track distance between two adjacent lines during the manufacturing process. This should be taken into account when creating the CAD model for the L-PBF process; i.e., for a desired slit width, a correspondingly higher nominal value of the slit width must be used for the CAD model.

Magnetic response investigation is a measurement method for qualitative comparison of the magnetic flux within the same or similar components. This allows conclusions to be drawn about the iron losses. The values obtained cannot be explicitly traced back to individual loss components but reflect the total losses.

The iron losses measured using the commercial measuring device are all normalized to the measured value of the compact component as built at 100 Hz. The reason for the normalized specification is the fact that, unlike a conventional measurement, the measurement setup is not a closed magnetic circuit and the ring geometries used for calculating  $H$  and  $J$  do not correspond to reality. Therefore, it cannot be assumed that the measured values also correspond to the actual losses. However, since the components have the same global dimensions among themselves, the results are comparable. Therefore, a qualitative statement can be made about the influence of the inserted slits and the heat treatment.

The integration of radially arranged slits leads to spatially lower eddy currents and thus to a lower proportion of eddy currents in the total losses. Therefore, the iron loss is highest in the component without slits. The higher reduction with wider slits is due to the fact that, in this case, there are fewer connection points along the slit, and the slit is relatively continuous, thus not allowing larger eddy currents. The narrow slits, on the other hand, are less continuous due to the manufacturing process, resulting in spatially larger eddy currents due to bridges between the slits. These results are consistent with other studies where the integration of slits oriented along the flux direction in 3%SiFe ring

samples also resulted in lower iron losses [23–27]. However, the slits in these studies are provided with several bridges due to mechanical stability and therefore not continuous.

The heat treatment reduces internal stresses and inhomogeneities in the microstructure. Furthermore, the grain structure is coarsened leading to a lower density of grain boundaries that generally act as pinning centers for domain walls and thus hinder the magnetization of the material. As a result, the proportion of hysteresis losses in the total losses decreases after the annealing. This effect was also observed by Tiismus et al. [23,24]. The reduction of iron losses by heat treatment has a somewhat greater effect on components without or with only narrow slits, since in these cases a larger contiguous defective magnet volume is restored or improved. However, restoration of the microstructure slightly reduces the resistivity of the material, which at high frequencies (outside the operating frequencies of the transverse flux machine) leads to increased eddy current losses and counteracts the lower hysteresis losses. For this reason, the heat treatment carried out is counterproductive from an excitation frequency of just over 1000 Hz, since from this frequency onwards the eddy current losses take on a significantly higher weighting and cancel out the improved hysteresis losses. As seen in Figure 9, the annealing process of the components has no effect on the thermal stability of the slits, so that an increase of the eddy current losses due to merging of the slits can be ruled out.

The percentage differences between the measurements can largely be attributed to the deviating target polarization, which is significantly lower in the case of the measurement with the commercial device at 0.1 T than in the magnetic response experiment. The reason for this is that, with the magnetic response setup, the correct current for an intended maximum polarization of up to 0.8 T can flow immediately and the measurement can be made within a very short time. The coil system experiences almost no significant heating in this setup. However, in the commercial instrument, it takes time for the correct current to build up to achieve the desired maximum polarization. During this time, the thin coil windings would already heat up too much and destroy the coil system. Therefore, a lower target polarization, at which a non-destructive operation of the coil system was guaranteed, was selected for this measurement method.

## 5. Conclusions

The investigations carried out as part of this study yielded the following results:

- Components of a transverse flux machine made of pure iron were successfully fabricated using additive manufacturing.
- In order to improve the magnetic behavior of the components, radial slits have been integrated. To obtain the narrowest possible but continuous slits, the specified slit width must be at least 250  $\mu\text{m}$ . The actual slit widths are smaller than predefined, mainly because of the deliquescence of the melt bath during the AM process. For nominal values of 150 and 300  $\mu\text{m}$ , actual slit widths of 0–100  $\mu\text{m}$  and 75–190  $\mu\text{m}$  have been achieved.
- A suitable heat treatment and the integration of radial slits significantly reduced the iron losses in the component.
- The reduction of iron losses is larger the fewer the connection points in the slits are. Wider slits in the component design thus lead to lower iron losses in the components. For example, the integration of slits, with nominal widths of 150 and 300  $\mu\text{m}$  in the annealed state in an alternating field with 0.1 T peak polarization and a frequency of 500 Hz, led to a reduction in volume-specific iron losses of 13% and 49%, respectively.

The component configurations presented can be further improved in the future. Once the effectiveness of the slit geometries integrated has been successfully demonstrated for the purpose of loss reduction, further optimization of the process parameters can be undertaken. For example, the parameters for different areas of the components can be chosen differently, which can result in a reduction of losses. If the flatness of the slit surfaces is improved, the slit width can also be reduced. This has the effect of increasing the proportion of soft magnetic material and thereby improving the magnetic properties, in

particular polarization. These results can in turn be used in the modeling of the ideal slit configuration to enable further optimization with respect to magnetic performance.

**Author Contributions:** Conceptualization, D.G., T.K. (Thomas Kresse), J.S., G.S., M.S. and N.P.; powder analysis, T.K. (Torsten Kunert); sample manufacturing and heat treatment, J.S. and T.K. (Torsten Kunert); magnetic response measurements, M.L.; microscopy, T.K. (Torsten Kunert); Brockhaus measurements, T.K. (Thomas Kresse); CT analyses, T.K. (Torsten Kunert), CAD conception, M.S.; writing—original draft preparation, T.K. (Thomas Kresse), J.S., D.G. and G.S.; writing—review and editing, D.G., T.K. (Thomas Kresse), G.S. and N.P.; supervision, D.G. and G.S.; project administration, D.G. and N.P.; funding acquisition, D.G. and N.P. All authors have read and agreed to the published version of the manuscript.

**Funding:** This research was funded by the Ministry of Science, Research and the Arts Baden-Württemberg (MWK) within the scope of the project TopoMAG (grant number: EM-1 TopoMAG) in the framework of ICM (InnovationsCampus Mobilität der Zukunft).

**Data Availability Statement:** Not applicable.

**Acknowledgments:** The authors gratefully acknowledge G. Martinek and F. Willburger (both Aalen University) for their support in setting up and performing measurements using the magnetic response method.

**Conflicts of Interest:** The authors declare no conflict of interest.

## References

1. Xie, J.; Pan, H.; Fu, H.; Zhang, Z. High Efficiency Warm-cold Rolling Technology of Fe-6.5wt%Si Alloy Sheets. *Procedia Eng.* **2014**, *81*, 149–154. [[CrossRef](#)]
2. Goll, D.; Schuller, D.; Martinek, G.; Kunert, T.; Schurr, J.; Sinz, C.; Schubert, T.; Bernthaler, T.; Riegel, H.; Schneider, G. Additive manufacturing of soft magnetic materials and components. *Addit. Manuf.* **2019**, *27*, 428–439. [[CrossRef](#)]
3. Wrobel, R.; Mecrow, B. Additive Manufacturing in Construction of Electrical Machines—A Review. In Proceedings of the 2019 IEEE Workshop on Electrical Machines Design, Control and Diagnosis (WEMDCD), Athens, Greece, 22–23 April 2019; pp. 15–22.
4. Garibaldi, M.; Ashcroft, I.; Simonelli, M.; Hague, R. Metallurgy of high-silicon steel parts produced using Selective Laser Melting. *Acta Mater.* **2016**, *110*, 207–216. [[CrossRef](#)]
5. Kallaste, A.; Vaimann, T.; Rassälkin, A. Additive Design Possibilities of Electrical Machines. In Proceedings of the 2018 IEEE 59th International Scientific Conference on Power and Electrical Engineering of Riga Technical University (RTUCON), Riga, Latvia, 12–13 November 2018.
6. Lammers, S.; Quattrone, F.; Ponick, B. Additive Manufacturing of a lightweight rotor for a permanent magnet synchronous machine. In Proceedings of the 2016 6th International Electric Drives Production Conference (EDPC), Nuremberg, Germany, 30 November–1 December 2016.
7. Metsä-Kortelainen, S.; Lindroos, T.; Savolainen, M.; Jokinen, A.; Revuelta, A.; Pasanen, A.; Ruusuvoori, K.; Pippuri, J. Manufacturing of topology optimized soft magnetic core through 3D printing. In Proceedings of the NAFEMS Exploring the Design Freedom of Additive Manufacturing through Simulation, Helsinki, Finland, 22–23 November 2016.
8. Garibaldi, M.; Gerada, C.; Ashcroft, I.; Hague, R. Free-Form Design of Electrical Machine Rotor Cores for Production Using Additive Manufacturing. *J. Mech. Design* **2019**, *141*, 71401. [[CrossRef](#)]
9. Plotkowski, A.; Pries, J.; List, F.; Nandwana, P.; Stump, B.; Carver, K.; Dehoff, R.R. Influence of scan pattern and geometry on the microstructure and soft-magnetic performance of additively manufactured Fe-Si. *Addit. Manuf.* **2019**, *29*, 100781. [[CrossRef](#)]
10. Andreiev, A.; Hoyer, K.-P.; Dula, D.; Hengsbach, F.; Haase, M.; Gierse, J.; Zimmer, D.; Tröster, T.; Schaper, M. Soft-magnetic behavior of laser beam melted FeSi3 alloy with graded cross-section. *J. Mater. Process. Technol.* **2021**, *296*, 117183. [[CrossRef](#)]
11. Gargalis, L.; Madonna, V.; Giangrande, P.; Rocca, R.; Hardy, M.; Ashcroft, I.; Galea, M.; Hague, R. Additive Manufacturing and Testing of a Soft Magnetic Rotor for a Switched Reluctance Motor. *IEEE Access* **2020**, *8*, 206982. [[CrossRef](#)]
12. Zhang, Z.Y.; Jhong, K.J.; Cheng, C.W.; Huang, P.W.; Tsai, M.C.; Lee, W.H. Metal 3D printing of synchronous reluctance motor. In Proceedings of the 2016 IEEE International Conference on Industrial Technology (ICIT), Taipei, Taiwan, 14–17 March 2016.
13. Kastinger, G. Design of a novel transverse flux machine. In Proceedings of the 2002 International Conference on Electrical Machines (ICEM), Bruges, Belgium, 26–28 August 2002.
14. Arshad, W.M.; Backstrom, T.; Sadarangani, C. Analytical design and analysis procedure for a transverse flux machine. In Proceedings of the IEEE International Electric Machines and Drives Conference (IEMDC), Cambridge, MA, USA, 17–20 June 2001; pp. 115–121.
15. Kaiser, B.; Parspour, N. Transverse Flux Machine—A Review. *IEEE Access* **2022**, *10*, 18395. [[CrossRef](#)]
16. Wan, Z.; Ahmed, A.; Husain, I.; Muljadi, E. A novel transverse flux machine for vehicle traction applications. In Proceedings of the 2015 IEEE Power & Energy Society General Meeting, Denver, CO, USA, 26–30 July 2015.

17. Guo, Y.G.; Zhu, J.G.; Watterson, P.A.; Wu, W. Development of a PM transverse flux motor with soft magnetic composite core. *IEEE Trans. Energy Convers.* **2006**, *21*, 426–434. [[CrossRef](#)]
18. Shokrollahi, H.; Janghorban, K. Soft magnetic composite materials (SMCs). *J. Mater. Process. Technol.* **2007**, *189*, 1–12. [[CrossRef](#)]
19. Keller, M.; Müller, S.; Parspour, N. Design of a permanent magnetic excited transverse flux machine for robotic applications. In Proceedings of the 2016 XXII International Conference on Electrical Machines (ICEM), Lausanne, Switzerland, 4–7 September 2016; pp. 1520–1525.
20. Keller, M.; Müller, S.; Parspour, N. Design of a transverse flux machine as joint drive for an articulated six-axis robot arm. In Proceedings of the 2016 International Symposium on Power Electronics, Electrical Drives, Automation and Motion (SPEEDAM), Capri, Italy, 22–24 June 2016; pp. 849–854.
21. Keller, M.; Parspour, N. Experimental identification and validation of model parameters of a permanent magnetic excited transverse flux machine for robotic applications. In Proceedings of the 2017 11th IEEE International Conference on Compatibility, Power Electronics and Power Engineering (CPE-POWERENG), Cadiz, Spain, 4–6 April 2017; pp. 352–357.
22. Kumar, S.; Czekanski, A. Optimization of parameters for SLS of WC-Co. *Rapid Prototyp. J.* **2017**, *23*, 1202. [[CrossRef](#)]
23. Tiismus, H.; Kallaste, A.; Belahcen, A.; Tarraste, M.; Vaimann, T.; Rassälkin, A.; Asad, B.; Ghahfarokhi, P.S. AC Magnetic Loss Reduction of SLM Processed Fe-Si for Additive Manufacturing of Electrical Machines. *Energies* **2021**, *14*, 1241. [[CrossRef](#)]
24. Tiismus, H.; Kallaste, A.; Vaimann, T.; Lind, L.; Virro, I.; Rassälkin, A.; Dedova, T. Laser Additively Manufactured Magnetic Core Design and Process for Electrical Machine Applications. *Energies* **2022**, *15*, 3665. [[CrossRef](#)]
25. Tiismus, H.; Kallaste, A.; Vaimann, T.; Rassälkin, A. State of the art of additively manufactured electromagnetic materials for topology optimized electrical machines. *Addit. Manuf.* **2022**, *55*, 102778. [[CrossRef](#)]
26. Tiismus, H.; Kallaste, A.; Naseer, M.U.; Vaimann, T.; Rassälkin, A. Design and Performance of Laser Additively Manufactured Core Induction Motor. *IEEE Access* **2022**, *10*, 50137–50152. [[CrossRef](#)]
27. Baco-Carles, V.; Huguet, T.; Llibre, J.-F.; Baylac, V.; Pasquet, I.; Tailhades, P. Laser powder bed fusion applied to the manufacture of bulk or structured magnetic cores. *J. Mater. Res. Technol.* **2022**, *18*, 599–610. [[CrossRef](#)]